Impulsive Flares: A Microwave Perspective

T. S. BASTIAN

National Radio Astronomy Observatory, Socorro, NM 87801, USA
E-mail: tbastian@nrao.edu

Abstract

Impulsive flares, by far the most common flares on the sun, impose strong demands on any theory of energy release and of particle acceleration. For a large flare, $\sim 10^{37}$ electrons with energies > 20 keV must be accelerated each second. These electrons produce hard X-rays by nonthermal bremsstrahlung emission and radio waves by plasma radiation processes and gyrosynchrotron emission. The hard X-ray emission is dominated by thick-target bremsstrahlung from fast electrons streaming directly from the acceleration site to the low corona and upper chromosphere, and by fast electrons precipitating from the magnetic trap. By contrast, microwave emission may be dominated by trapped electrons.

In this paper, I briefly discuss the basic properties of microwave emission from impulsive flares: its morphology, source kinematics, and its relation to emissions at other wavelengths. I then summarize diagnostic uses of microwave emission and conclude with a description of recent work on the problem of the relative timing of HXR and microwave emission. It is shown that magnetic loops act as dispersive elements, allowing fixed-frequency observations to be used to probe electrons of differing energy. Spatially and temporally resolved observations of gyrosynchrotron emission from solar flares, such as those available from the Nobeyama Radioheliograph, enable one to constrain the evolution of the electron distribution function in time. I discuss some results of a comparative timing analysis of a sample of flares observed by the Nobeyama Radioheliograph and by the CGRO BATSE instrument.

Key words: Sun: Flares – Sun: Radio Radiation – Sun: X-rays – Acceleration of Particles – Turbulence

1. Introduction

Radio emission from solar flares divides itself naturally into two wavelength regimes. At wavelengths $\lambda \gtrsim 10$ cm ($\nu \lesssim 3$ GHz), flare-associated radio emission is often dominated by coherent plasma radiation from beams of non-thermal electrons (type III bursts), continuum emission due to plasma and/or gyrosynchrotron radiation (type IV or "flare continuum" radiation), and plasma radiation driven by flare-associated MHD shocks (type II bursts). Reviews of decimeter and meter wavelength emission appear elsewhere in this proceedings (see the papers of Aschwanden, Aurass, Pick, and Melrose). At wavelengths $\lambda \lesssim 10$ cm ($\nu \gtrsim 3$ GHz), coherent emission processes become relatively unimportant and flare-associated radio emission is dominated by incoherent gyrosynchrotron emission from thermal or nonthermal populations of energetic electrons, and thermal free-free emission.

The centimeter wavelength range (microwaves) is particularly interesting as a diagnostic of physical parameters and processes during flares and will be the focus of this paper. This is because incoherent gyrosynchrotron emission typically dominates the emission, at least during the impulsive phase of flares. Incoherent gyrosynchrotron emission is due to the interaction of energetic electrons with the magnetic field. At centimeter wavelengths, the energy of the emitting electrons ranges from some 10s of keV to ~ 1 MeV. These electrons are of particular interest because they carry a significant fraction of the energy released during the impulsive phase, although recently it has been recognized that ions with energies greater than 1 MeV/nucleon play a comparable, and sometimes a dominant, role in gamma-ray line (GRL) flares (see Vilmer, this proceedings). Gyrosynchrotron emission from energetic electrons provides a diagnostic tool with which to constrain the evolving electron distribution function, the magnetic field in the source, and properties of the ambient plasma.

This review is divided into three parts. In the first, I review the observational properties of flare-associated microwave emission. A much more exhaustive discussion of the observations is availble in a lengthy review by Bastian, Benz, & Gary (1998). In the second part I briefly summarize some of the diagnostic uses of microwave observations, including some of a more speculative nature. I end with a description of recent work on the relative timing of microwave and hard X-ray (HXR) emission and some discussion of its possible implications for electron acceleration and transport.
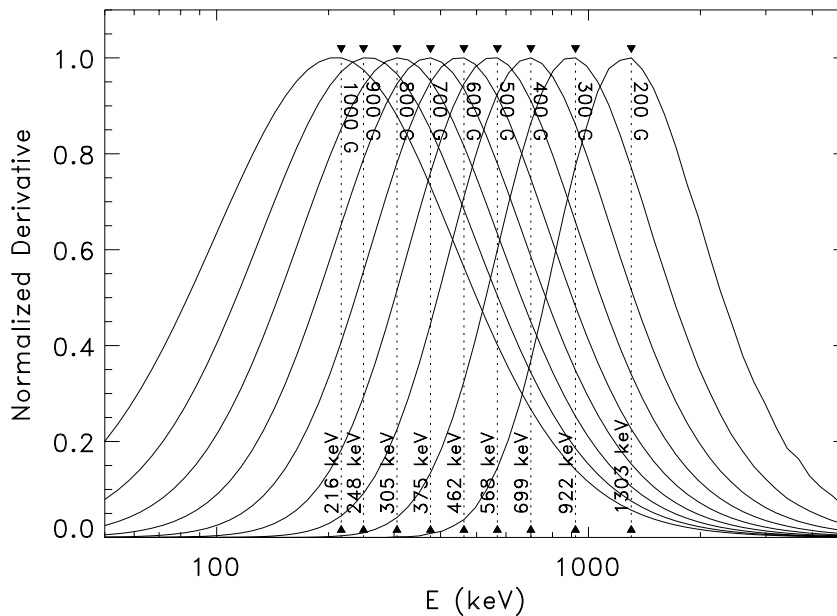
Fig. 1.. Normalized contribution functions to 17 GHz emission from a power-law distribution of electrons with a spectral index $\delta = 4$ as a function of magnetic field strength. The source is homogeneous.

2. Microwave Source Properties

2.1. Emission Mechanism and Electron Energy

Flare-associated radio emission at centimeter and millimeter wavelengths is dominated by incoherent gyrosynchrotron emission during the impulsive phase of flares (see White, this proceedings, for a discussion of millimeter wavelength emission). It has long been assumed that, because the time profiles of HXR and microwave emission are so similar (Kundu 1961) and because of the tight correlation between peak fluxes in the two emissions (e.g., Kosugi, Kai, and Dennis 1988), the "same" electrons are responsible for the two emissions. This is true to first order, but some qualifications should be mentioned. First, if by HXR emission we mean photon energies $\lesssim 100$ keV, the energy of the relevant electrons, presumed to emit by nonthermal thick-target bremsstrahlung, have energies $\lesssim 200$ keV. The energy of microwave-emitting electrons depends on the frequency observed and on the magnetic field strength and its orientation in the source. At frequencies $> 10 - 20$ GHz, which are typically optically thin, the emission is due to electrons with energies between 200 keV to ~ 1 MeV (Figure 1). Second, HXR emission is dominated by footpoint emission from electrons streaming down from the corona. This is not necessarily the case for microwave emission – there can be a significant coronal component to the emission (see §3). Hence, while drawn from the same population of energetic electrons, the source regions and the relevant electron energies can differ for HXR and microwave emission.

2.2. Source Morphology

As is the case for EUV and X-ray sources, the basic morphological element of flare-associated microwave sources is a "loop", corresponding to a coronal magnetic loop. On the basis of radio imaging observations alone, it is not always obvious that this is the case. Figure 2 shows a schematic model where an asymmetric magnetic loop containing a power-law, isotropic distribution of nonthermal electrons emits via the gyrosynchrotron mechanism. The source morphology changes dramatically as the emission is computed for a progression of frequencies. When the source is optically thick, the maximum intensity occurs between the magnetic footpoints. As the source becomes optically thin at high frequencies, emission near the footpoints dominates. The polarization of the loop (not shown) is in the sense of the extraordinary mode for optically thin emission; i.e., right-circularly polarized for the footpoint with positive
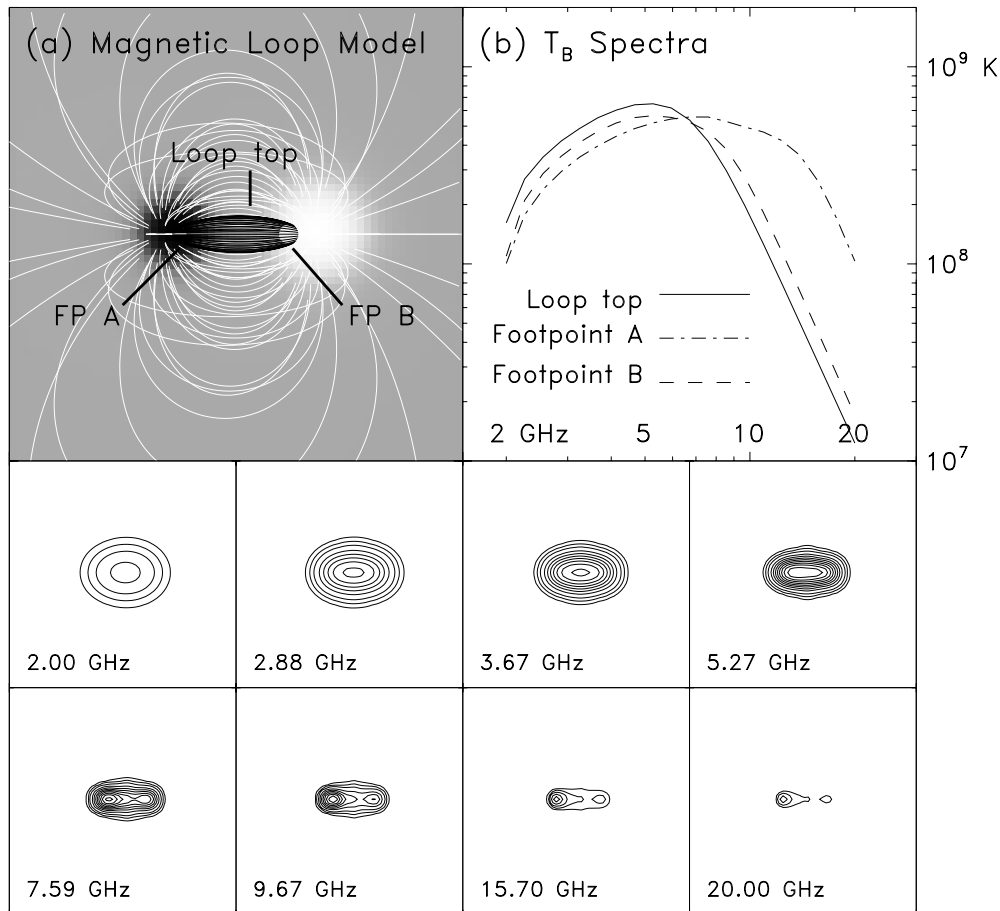
Fig. 2.. The distribution of gyrosynchrotron emission from a model coronal magnetic loop containing an isotropic, power-law distribution of energetic electrons. (a) The model configuration. The magnetic field is defined by two solenoids. The longitudinal component of the magnetic field is shown in greyscale. Footpoint A has a magnetic field strength of -1000 G and footpoint B is +500 G. White lines show a sampling of lines of force and black lines define the half-width of the spatial distribution of energetic electrons, taken to be a Gaussian in cross-section. The spectral index of the electron distribution is $\delta = 4$ and the number density of electrons with an energy > 10 keV is taken to be 5×10^6 cm^{-3} on the loop axis. (b) Brightness temperature spectra at the locations indicated in panel (a). The bottom two row the brightness distribution of the total intensity is shown in eight frequencies. The contour levels are $2\%, 5\%, 10\%, 20\%, 30\%, 40\%, 50\%, 60\%, 70\%, 80\%, and 90\%$ of 6×10^8 K. The scale of the lower panels is half that of (a) and (b). From Bastian, Benz, and Gary (1998).

magnetic polarity. The schematic model also includes the effects of an ambient plasma. The free-free absorption is relatively insignificant, but Razin-Tsytovich suppression plays a role below $\nu \approx 2$ GHz for the background density of 3×10^{10} cm^{-3} (see §3.5). Note that harmonic structure in the gyrosynchrotron brightness temperature spectra, which is typically seen in homogeneous source models, is washed out by gradients in the magnetic field. Similar calculations have been performed by Klein & Trottet (1984) and by Preka-Papadema & Alissandrakis (1992).

Observations show more complex source morphologies, of course, because they are generally composed of multiple magnetic loops. Figure 3 shows an example of the GOES M1.9 flare observed by the VLA at 15 GHz with an angular resolution of $\approx 4''$. Here, clearly, the source is composed of two parallel magnetic loops or loop systems, both of which were active during the course of the flare.

2.3. Relation to Optical and X-ray Sources

The relation of microwave sources to HXR, soft X-ray (SXR), Hα emission, and magnetograms, and its implications for energy release, is discussed by Hanaoka and by Nishio elsewhere in this proceedings (see also Hanaoka 1996, 1997; Nishio et al. 1997). Briefly, microwave sources indicate those locations where energetic electrons are present. At
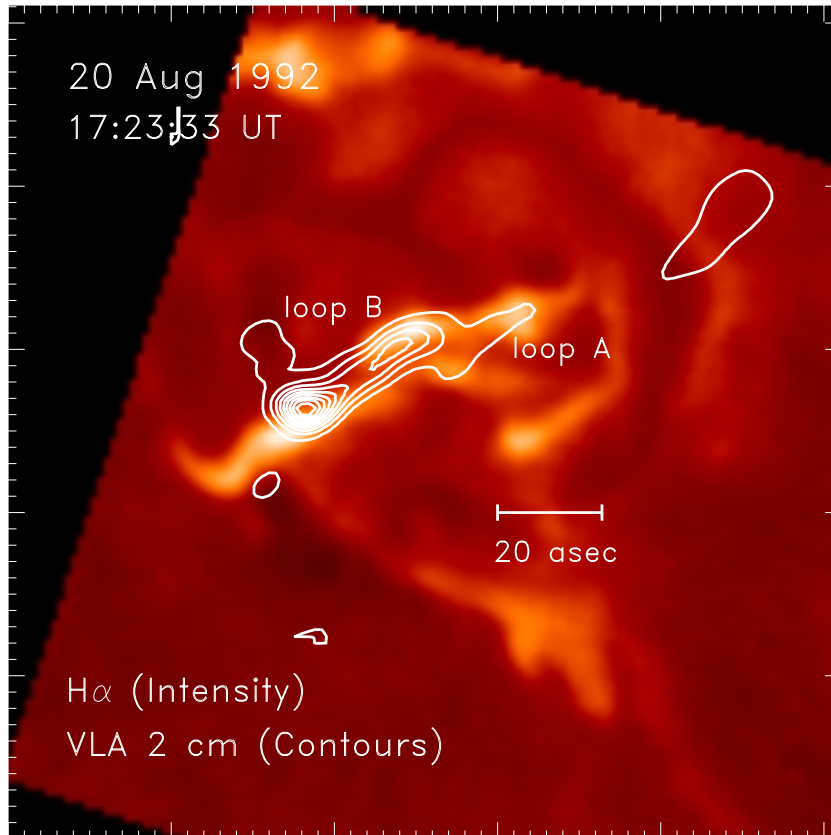
Fig. 3.. VLA observation of a GOES M1.9 flare on 20 Aug 1992. The array was in the D configuration, yielding an angular resolution
of $4''$. There are two parallel loops or loop systems joining the two Hα ribbons (loops A,B). Early in the event an impulsive spike
originated in the loop A. At the time shown, the loop B is active. Note the similarity between the loop B and the (optically thin)
model sources shown in Fig. 2.

high frequencies, microwave emission from conjugate sets of magnetic footpoints is favored and a close relationship
between microwave footpoint sources and HXR footpoint sources is expected. Such a relationship is, in fact, observed
(Wang et al. 1995; Kundu et al. 1995).

Some qualifications are in order, however. For an asymmetric magnetic loop, optically thin gyrosynchrotron
emission is strongly weighted by the magnetic field strength and orientation: roughly as $\eta_{gs} \propto B^{0.9\delta-0.22} \sin\theta^{-0.43+0.65\delta}$
for a power-law distribution of electrons, where η_{gs} is the gyrosynchrotron emissivity and θ is the angle between
the line of sight and the magnetic field vector (Dulk 1985; Preka-Papadema & Alissandrakis 1988). The stronger
magnetic footpoint can be brighter than its conjugate footpoint. Indications are that the opposite is often true in
HXR emission: the magnetically weaker footpoint emits more strongly because electron precipitation is favored there
(Wang et al. 1995; Kundu et al. 1995). Hence, there can be a spatial separation between the dominant HXR source
and the dominant microwave source. At times the relationship between high frequency microwave footpoint emission
and HXR footpoint emission is unclear owing to the complexity of the source and/or limited angular resolution. In
some cases the presence of polarization gradients in poorly resolved microwave sources can help to disentangle the
underlying source structure, as pointed out by Hanaoka (1996, 1997).

At lower frequencies, a significant area of the source may be optically thick, thereby illuminating entire magnetic
loops or loop systems. Optically thick emission may bear little resemblance to the HXR emission. An example of
an optically thick microwave source is shown in Figure 4. While impulsive flares are emphasized here, the example
shows a long duration event that was observed on 17 June 1989 by the VLA in its C configuration (Bastian and
Kiplinger 1991) at a frequency of 4.9 GHz ($\lambda = 6.1$ cm) and an angular resolution of $\approx 5''$. The fourth panel
corresponds to the time of the maximum radio emission, when the source is optically thick over most of its extent.
It spans the magnetic neutral line, connecting an arcade of magnetically conjugate footpoints. It is interesting to
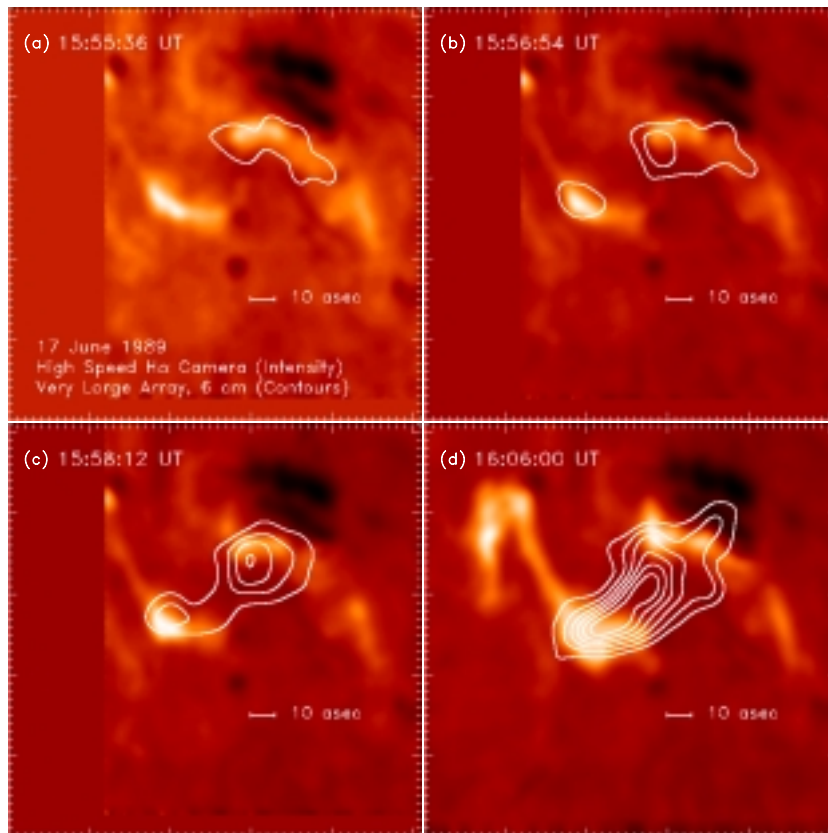
Fig. 4.. An example of the time evolution of a flaring source at centimeter wavelengths. The contours show the 6 cm emission observed by the VLA (C configuration) with an angular resolution of $4''$. The background shows the corresponding Hα emission. Large sunspots are seen to the northwest. The flare was an M8.9 LDE accompanied by a CME and was discussed by Bastian & Kiplinger (1991). (a) Early in the flare, the region containing the strongest magnetic fields is illuminated. (b) The magnetically conjugate footpoint then emits. (c) The magnetic neutral line is then bridged with emission. (d) The entire 6 cm source is optically thick near the time of the flare maximum and the maximum source brightness lies between the footpoints.

note that the length of the Hα ribbons is far greater than the lateral extent of the microwave source. The spatial extent of the most energetic electrons is smaller than the lower energy electrons and/or heating responsible for the Hα emission in the chromosphere.

2.4. Source Kinematics

Microwave sources are highly time variable in their flux, polarization, spectrum, and morphology. Three factors contribute to time variability: 1) changes in optical depth caused by variations in the electron number density and/or the electron distribution function; 2) the dominant emission and absorption mechanisms may change as a function of time; 3) the magnetic connectivity of the source may change as a result of flux emergence, magnetic reconnection, or both. Consequently, different magnetic loops may contain fast electrons at different times. An example of dramatic variations in the source morphology in response to changes in the optical depth of the source is presented in Figure 4. Early in the flare, only the strongest magnetic fields, those in close proximity to the large sunspots to the northwest, are seen in the 4.9 GHz emission. The number of energetic electrons increases with time, increasing the optical depth of the conjugate footpoints to the southwest. The neutral line is then bridged as the number density of electrons continues to increase until, finally, the magnetic loops containing the most energetic electrons are rendered optically thick along their entire length.

3. Diagnostic Uses of Microwave Emission

The diagnostic uses of gyrosynchrotron emission from flares are numerous, but have remained underexploited. This is because its use as a diagnostic requires:

- Spatially resolved observations of the source, ideally with an resolution sufficient to resolve all emitting elements ($\sim 1''$).

- Full frequency coverage over the microwave band and higher, in order to measure the brightness temperature spectrum at each location in the source.

- Good time resolution ($\Delta t < 1$ sec) in order to resolve source kinematics.

- Measurements of the Stokes I and V polarization parameters.

Even with "ideal observations" in hand, a substantial modeling effort is often required to extract the information of interest. Unfortunately, no telescope provides ideal observations. The VLA can only provide high-resolution imaging at one or two frequencies on an occasional basis. The OVRO Solar Array provides good spectral coverage, but poor imaging capabilities. The Nobeyama Radioheliograph provides imaging at 17 and 34 GHz with a time resolution as high as 100 ms, but the angular resolution is typically $10 - 20''$ and $5 - 10''$, respectively. Nevertheless, working within the limitations imposed by current instrumentation, progress has been made in deducing physical quantities and physical processes from microwave observations of flares.

3.1. Constraints on Energy Release

It is worth emphasizing that microwaves trace out those magnetic loops in the solar corona to which energetic electrons have access. The papers of Nishio and of Hanaoka in this proceedings explore some of the implications of microwave source morphology for energy release. Previous work in SXR imaging (e.g., Kahler 1977 and, more recently, Sakurai et al. 1992) has shown changes in magnetic field topology, as traced out by thermal, SXR-emitting plasma, before and after a flare. Such work suggests that the magnetic field relaxes from a nonpotential configuration to a more nearly potential configuration. Such studies are ambiguous, however, because it is not clear that the same field lines are traced out by hot plasma before and after a given flare. Furthermore, the bulk of the thermal plasma is a by-product (energy release $\longrightarrow$ electron energization $\longrightarrow$ electron transport $\longrightarrow$ electron thermalization) of the primary processes of interest (energy release, electron acceleration, electron injection). Microwave emission from nonthermal electrons provides a more direct tracer of the magnetic loops involved in energy release at any given time during the course of a flare.

3.2. Direct Measurement of the Energy of the Emitting Electrons

One of the most straightforward observations with an imaging instrument operating at centimeter wavelengths is to measure the brightness temperature of the flaring source at an optically thick frequency. For a uniform source, the brightness temperature is related to the effective temperature of the emitting electrons by $T_B = T_{eff}(1 - e^{-\tau_{gs}})$, where τ_{gs} is the optical depth of the source to gyrosynchrotron absorption. If $\tau_{gs} \gg 1$, $T_B = T_{eff}$ and the mean energy of the emitting electrons at the relevant frequency is $\langle E \rangle = k_B T_{eff}$. Past observations of such measurements are summarized by Bastian, Benz, and Gary (1998) which yield mean energies of several tens to several hundreds of keV.

3.3. Constraints on the Electron Distribution Function

More importantly, with broadband frequency coverage, the microwave spectrum and its evolution in time can be observed. As mentioned previously, no instrument currently provides the necessary combination of angular and temporal resolution along with the broadband spectral coverage. However, the OVRO solar array, which samples 45 frequencies between 1-18 GHz with a time resolution of 12 s, has an imaging capability sufficient to show tantalizing differences in the spectra at the footpoints of flaring loops compared with those obtained near the loop top. Wang et al. (1994) present an observation of a flare for which the microwave spectrum of the footpoint is a power law. The spectral index of the power-law distribution of microwave-emitting electrons matches that derived from the HXR footpoint emission observed by the BATSE instrument on board the *Compton Gamma Ray Observatory* (CGRO). In contrast, the spectrum of the loop top is more consistent with *thermal* gyrosynchrotron emission. An alternative

possibility is that the electron distribution at the loop top was highly anisotropic (pancake pitch angle distribution), which would suppress the high-frequency emission and produce a steep spectrum (Ramaty 1969).

With good angular resolution and frequency coverage, such studies could be taken much further, of course. The spectrum and hence, the electron distribution function, could be parameterized at each location in the source. Such spectra could easily track the time evolution of the spectral index of a power-law electron distribution as a function of time and location, and the presence or absence of additional spectral components (e.g., a second power-law component). Such measurements could place powerful constraints on electron acceleration mechanisms (§3.6 and §4).

3.4. Magnetic Field Measurements

The spectral turnover frequency, the frequency where the microwave spectrum makes the transition from optically thin emission to optically thick emission, is a sensitive function on the magnetic field strength and orientation. An approximate expression for the turnover frequency ν_{pk} of the extraordinary mode emitted by an isotropic power-law distribution of nonthermal electrons emitting in a uniform source is given by Dulk (1985) as:

$$\nu_{pk} = 2.72 \times 10^3 10^{0.27\delta} (\sin\theta)^{0.41+0.03\delta} (NL)^{0.32-0.03\delta} B^{0.68+0.03\delta}$$

where δ is the power-law index, N the number of energetic electrons with an energy $E > 10$ keV, L the thickness of the source, θ the angle of the line of sight to the magnetic field vector, and B the magnetic field strength. Spatially unresolved observations of flare-associated emission have used this or similar expressions to infer the mean magnetic field in the emitting source for many years. More recently, observed spectra have been fit to those computed using the formalism of, e.g., Ramaty (1969), for the gyrosynchtron emission and absorption coefficients.

With spatially resolved spectroscopy, the magnetic field can be inferred along each line of sight in the source. This sort of "coronal magnetography" would provide a more direct means of constraining the magnetic field strength and orientation from place to place within the flaring source. Microwave spectroscopy is unique in this capability. A means of constraining the positional dependence of the magnetic field strength, independent of its orientation or of the electron distribution function is outlined in §4.1.

3.5. Constraints on the Ambient Plasma Density

At low frequencies, in the presence of a magnetized plasma, gyrosynchrotron emission is reduced by Razin-Tsytovich suppression. It occurs below a frequency $\nu_{RT} \lesssim \nu_{pe}^2/\nu_{Be} \approx 14 n_{th}/B$, where $\nu_{pe} = e^2 n_{th}/\pi m_e$ is the electron plasma frequency and $\nu_{Be} = eB/2\pi m_e c$ is the electron gyrofrequency. It manifests itself as a low-frequency cutoff in the spectrum (see Fig. 2). With the magnetic field strength deduced from the spectral turnover, the ambient plasma density can then be deduced along each line of sight from ν_{RT}. By way of illustration, if the ν_{RT} is 4 GHz along a line of sight for which a magnetic field strength of 350 G is deduced, the mean plasma density would be $n_e \approx 10^{11}$ cm^{-3}. The use of temporally and spatially resolved observations of ν_{RT} might prove to be a valuable diagnostic of thermal plasma in the flaring source because it is sensitive to plasma of all temperatures. In this sense, it is complementary to SXR observations of thermal plasma in flaring sources.

3.6. Constraints on Electron Acceleration and Transport

A problem of fundamental importance in the physics of flares is understanding the acceleration, injection, and transport of energetic electrons. For the remainder of this paper, I will outline some recent work in this area. Specifically, I will discuss work on the relative timing of microwave and HXR emission and its implications for the acceleration and transport of electrons.

4. The Relative Timing of Microwave and HXR Emission

As discussed in §2.1, the similarity between HXR and microwave light curves and the correlation between peak fluxes in the two emissions is a result of the fact that the emitting electrons are drawn from the same population of electrons. Yet the two emissions differ in detail. Imaging observations have demonstrated that the they are not necessarily cospatial; nor are they the result of electrons with the same energy (§2). In addition, timing observations have demonstrated that the microwaves are delayed with respect to HXR emission by a fraction of a second to a few seconds (e.g., Figure 5).

One way to account for the observed microwave delay is to suppose that that electron trapping is significant (e.g., Kauffmann 1983, Cornell *et al.* 1984, Dennis 1988). For fast electrons injected into a magnetic trap of constant ambient density, the high-energy electrons have a longer lifetime against Coulomb collisions than low-energy electrons do. Hence, the energetic electrons responsible for the microwaves remain in the coronal loop longer and the microwave emission they emit peaks later than the HXR emission, which is due to lower energy electrons. There are other possibilities, of course: thermal gyrosynchrotron or thermal bremsstrahlung emission may make an additional contribution to the microwave emission, thereby causing an apparent time difference between microwaves and nonthermal HXRs. Another possibility is that higher energy electrons are accelerated later than lower energy electrons (so-called "second-step" acceleration models; e.g., Bai and Ramaty 1979, Bai and Dennis 1985, Bai and Sturrock 1990).

Previous studies of microwave/HXR delays have employed spatially unresolved data. Crannell et al. (1978) cross correlated the total flux with HXR count rates and found a broad distribution of both positive and negative delays. The average delay of microwaves relative to HXRs was 2 sec, however. Cornell et al. (1984) performed a similar study, but applied a high-pass filter to the time series of data before cross correlation. They found a relatively tight distribution of delays, with a mean delay of microwaves to HXRs of 0.25 sec, an order of magnitude smaller than that of Crannell et al.

Bastian et al. (1999) have returned to the problem of microwave/HXR delays. The difference between their study and previous studies is that spatially-resolved microwave data are available from the Nobeyama Radioheliograph. Hence, specific locations within the microwave source can be isolated and cross-correlated with HXR light curves. Flares were selected for analysis on the basis of instrument coverage: they were observed by the Nobeyama Radioheliograph (17 GHz), the CGRO/BATSE instrument, and by *Yohkoh*. Of these, a heterogeneous sample of ten flares observed between 1992-1994 was selected for analysis. Briefly, light curves were constructed from the integrated flux and along discrete lines of sight from the 17 GHz data. These were compared with the 25–50 keV count rates from the BATSE instrument on board the CGRO. The light curves were first normalized to a maximum flux, or count rate, of unity. The cross-correlation coefficient (CCC) was then computed as a function of delay, its maximum corresponding to the appropriate delay. The CCC was computed as a function of delay for both the normalized light curves and for light curves first passed through a high-pass Fourier filter with a characteristic time scale of 10 sec. Further details can be found in Bastian et al. (1999). The results of this study may be summarized as follows:

1. As pointed out in §2, flare-associated microwave sources are often complex. Cross-correlations with spatially integrated 17 GHz light curves result in HXR/microwave delays that are seriously biased by the presence of multiple emitting components. Consequently, cross-correlations between HXRs and specific 17 GHz lines of sight curve can be strongly position dependent.

2. For those locations in the flaring source where the 17 GHz emission is closely correlated with the HXR emission, the 17 GHz emission is delayed relative to the HXR emission. Interestingly, for those cases where discrete coronal magnetic loops can be identified, the 17 GHz emission from the loop top is delayed relative to HXRs to a greater degree than are the foot points, and the more weakly magnetized footpoint is delayed to a greater extent than the more strongly magnetized footpoint.

The first result highlights the importance of imaging data: in the presence of multiple emitting components – e.g., loop top and footpoint sources – care must be exercised to compare the appropriate lines of sight with HXR data. The second result is illustrated in Figure 5 where a comparison of integrated and line-of-sight 17 GHz light curves with the CGRO/BATSE 25–50 keV HXRs is shown. All of the radio light curves are delayed relative to the HXRs. In the case of the first peak of the 7 Oct 1992 flare, the integrated 17 GHz flux is delayed 2.46 sec relative to the HXR emission. The RCP footpoint (A) is delayed by 2.16 sec and the LCP footpoint (B) is delayed by 2.70 sec. In the case of 23 Dec 93, the integrated 17 GHz flux is delayed 0.41 sec; the RCP footpoint (A) is delayed by 0.32 sec and the LCP footpoint is delayed by 2.22 sec. In order to understand the second result, I briefly digress to discuss the dispersive nature of magnetic loops.

4.1. *The Coronal Magnetic Loops as Dispersive Elements*

For a power-law, isotropic, distribution of energetic electrons, the mean energy $\langle E \rangle$ of the electrons emitting at a given frequency $\nu_\circ$ depends on the magnetic field strength as $\langle E \rangle \propto B^{-(0.5+0.085\delta)}$ (Dulk 1985), where δ is the spectral index of the electron distribution function (Figure 1). The magnetic field in a coronal loop is necessarily inhomogeneous, varying as a function of position along the loop. The field strength at the loop top is weaker
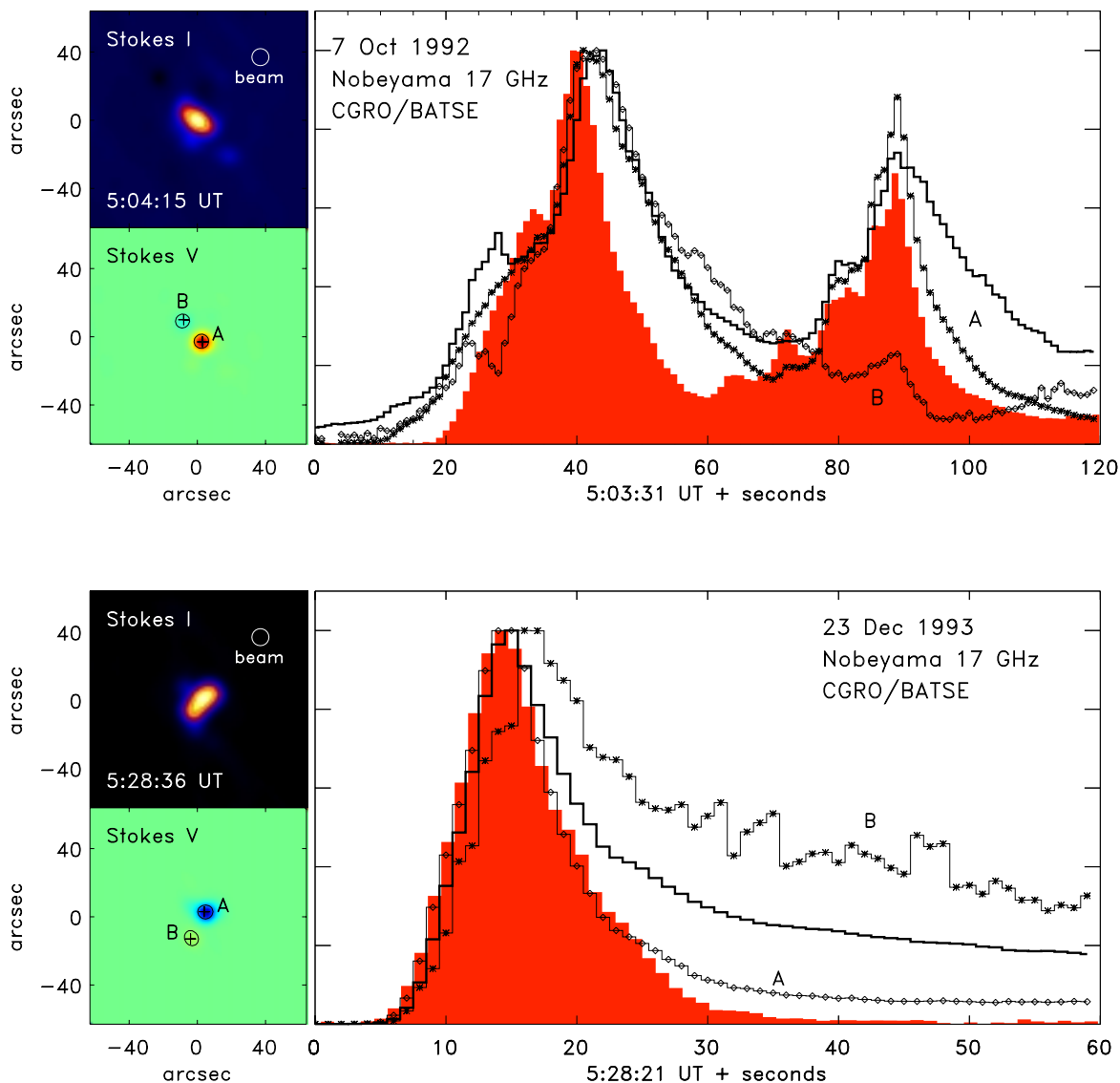
Fig. 5.. Two simple flares observed by the Nobeyama Radioheliograph and the BATSE instrument on the CGRO. In the top panel, the M3.1 flare on 7 Oct 1992 is shown. In the lower panel, the C4.4 flare on 23 Dec 1993 is shown. In both cases, snapshot maps of the total 17 GHz intensity and of the circularly polarized flux are shown to the left at the time indicated. To the right, normalized light curves are shown. The heavy solid line shows the profile of the integrated 17 GHz flux. Light curves obtained at the two magnetic footpoints are also shown. The shaded light curve shows the normalized CGRO/BATSE 25–50 keV count rate. The radio light curves are all delayed by varying degrees relative to the HXRs.

than at the footpoints. Consequently, if gyrosynchrotron emission is observed from a magnetic loop at a fixed frequency, $\nu_\circ$, the radiation from the footpoints originates from lower energy electrons than that from the loop top. A coronal magnetic loop therefore acts as a dispersive element: radiation from different parts of the loop is emitted by electrons with different mean energy. This is readily apparent in Figure 2b, where brightness temperature spectra corresponding to both foot points and the loop top are shown. At any given frequency on the optically thick side of the spectra the brightness temperature of the loop-top is greater than that of either magnetic foot point indicating that the mean energy of the emitting electrons is greater there.

It is interesting to note in passing that broadband imaging-spectroscopy offers a means of constraining the magnetic

field strength in flaring coronal loops (§3.4). Emission by electrons of a fixed energy corresponds to emission by electrons at a fixed harmonic s of the electron gyrofrequency $\nu_{Be} = eB/2\pi m_e c$. That is, we have $s = \nu/\nu_{Be} = const$. Since B varies as a function of position along a magnetic loop, so must ν. If one can measure the positional dependence of ν such that $s = const$, one has measured the positional dependence of the coronal magnetic field strength! How does one obtain ν such that $s = const$? Consider (optically thin) radio emission from two different positions along a coronal magnetic loop, r_1 and r_2, such that $B(r_1) > B(r_2)$. Then electrons with the same energy at the two positions emit at the frequencies $\nu_1 < \nu_2$. The *timing* of emission at ν_1 and ν_2 will be identical if they are due to electrons of the same energy. An absolute calibration of the magnetic field strength requires spectral fitting of the kind described in §3.4, perhaps at the polarization inversion where $theta = 90°$ and the angular dependence of the spectral turnover is unity. Hence, a measure of the magnetic field strength, independent of its orientation, is available in principle.

4.2. *Discussion of the Microwave/HXR Timing Results*

Given that coronal magnetic loops act as dispersive elements, the mean energy of electrons emitting at a fixed frequency varies as a function of position in the flaring source as a result of the magnetic field variation with position. Our timing study indicates that lines of sight to locations where the magnetic field is low are delayed to a greater extent than those lines of site to where the magnetic field is high, implying that the 17 GHz emission from higher energy electrons is delayed relative to that from lower energy electrons. Therefore, the main result of the timing study is that the electron distribution function hardens up to the time of maximum at microwave-emitting energies ($\sim 200 - 1000$ keV). Although this result was obtained in a novel way, it is not new, at least in qualitative terms. It has been known for decades that HXR emission typically displays a "soft-hard-soft" or "soft-hard-harder" spectral evolution.

Aschwanden et al. (1997a, b) have recently considered electron transport in the limit of weak diffusion as a convenient framework for analyzing HXR bursts. While a rigorous treatment of the transport problem requires solving the Fokker-Planck equation with the relevant physics and boundary conditions included, it is assumed that i) electron acceleration and injection are decoupled from transport; ii) transport is dominated by the mirror force and Coulomb collisions; iii) thin-target emission – i.e., energy loss in the corona – may be neglected. Under these assumptions, transport can be described by a trap model with precipitation and without energy losses. Two populations of electrons then contribute to HXR emission: those which have small pitch angles at injection and precipitate directly to the footpoints where they emit HXRs (DP electrons), and those with large enough pitch angles that they remain trapped for a time until Coulomb collisions on the ambient plasma scatter them to a small pitch angle and they precipitate (TPP electrons).

For a $\delta-$function injection of electrons in the corona, the high energy DP electrons reach the magnetic foot points before lower energy DP electrons. High-energy HXR emission from DP electrons therefore *leads* low-energy HXR emission from DP electrons (see Aschwanden, Schwartz, and Alt 1995; Aschwanden & Schwartz 1996; Aschwanden et al. 1996a, 1996b). In contrast, the time a TP electron remains in the trap before precipitating is roughly the Coulomb deflection time: $t_D \approx 0.95 \times 10^8 E_{keV}^{3/2} n_{th}^{-1}(20/\ln \Lambda)$, where $\ln \Lambda$ is the Coulomb logarithm. The energy dependence is such that more energetic electrons remain in the trap longer than less energetic electrons. HXR emission from high-energy TP electrons is therefore expected to *lag* that from low-energy TP electrons.

Aschwanden & Schwartz (1996) have exploited the timing features (time of flight) of the DP electrons to deduce the distance for the HXR source to the electron injection site. Aschwanden et al (1996) then considered the TP component separately and were able to constrain the ambient density in the trap by fitting the HXR timing to the expected $E^{3/2}$ dependence of the electron deflection time. Finally, Aschwanden et al (1997a,b) treat the DP and TP components jointly and, with the assumptions outlined above, are able to solve for physical parameters of interest – the ambient density, the electron trapping ratio and hence, the ratio of the magnetic field in the foot point to that at the electron injection – more self-consistently via an iterative deconvolution procedure.

Given the success of the DP+TPP/weak diffusion model in accounting for many of the features of the time variability of HXR emission, an obvious question to ask is whether the microwave/HXR timing observations can also be understood in terms of the same model? The 17 GHz emission is the result of more energetic electrons than is the HXR emission. Furthermore, in the weak diffusion model, microwaves are dominated by electrons trapped in coronal magnetic loops (TR electrons). That is, HXRs are emitted by DP+TPP electrons while microwaves are emitted predominantly by TR electrons. The fractional contribution of precipitating electrons to the observed emission is low because their pitch angles are small and their number density is small compared to the TR component. Therefore, the 17 GHz offers a means of probing the TR electrons more directly than HXR emission from TPP electrons, and

more importantly, a means of probing higher energy electrons than is possible with existing HXR spectroscopic and imaging instruments.

Few flares studied so far lend themselves to a joint HXR/microwave modeling effort because they are typically complex. However, two flares are distinguished by their simple morphology and by their simple emission profiles: those on 7 Oct 1992 and 23 Dec 1993 (Figure 5). A third flare (27 Oct 92), while more complex, will also be modeled because it is well-resolved by the radioheliograph and discrete loop components can be isolated. The 23 Dec 93 flare has been modeled, the details of which will be presented in Bastian & Aschwanden (1999). Briefly, we have modeled this flare as a single magnetic loop with a position, orientation, and magnetic field strength similar to that observed. The modeling proceeded in two parts. First, the HXR deconvolution scheme of Ascwhanden et al (1997b) was used to obtain the ambient density of plasma in the magnetic loop and the injection profile of energetic electrons, under the assumptions inherent to the method. The background density essentially fixes the Coulomb deflection time in the loop. The 17 GHz gyrosynchrotron emission and its time variation was then computed for a range of plausible magnetic parameters, guided by available magnetographic observations.

Our findings indicate that even with relatively extreme values of the magnetic field (hence, probing lower energy electrons), the model microwave emission is delayed by factors 3-5 times the observed values. There are several reasons why this might be the case. First, the flare, while simple, may not be well modeled by a single dominant loop. The fact that it's observed morphology is simple may be a result of inadequate angular resolution. If additional magnetic loops are present, then different lines of sight are not necessarily coupled to the same magnetic loop. However, if a single loop does indeed dominate the microwave emission, then the delays are inconsistent with the notion that Coulomb losses drive precipitation losses of electrons at microwave-emitting energies. Clearly, additional cases must be analyzed before firm conclusions can be drawn.

Continuing in a speculative vein for a moment, let us suppose that microwave observations do indeed probe an energy regime where Coulomb collisions no longer play a dominant role in electron transport. What transport process or processes account for the microwave delays and decay profiles? An attractive possibility is resonant wave-particle interactions. Such interactions can not only provide the necessary pitch-angle scattering needed for electron precipitation, but can also stochastically accelerate electrons to high energies (e.g., Hamilton & Petrosian 1992; see also Miller et al. 1997 for a broader discussion).

The implications of this idea are several: 1) while the DP+TPP model in the weak diffusion limit may be appropriate for electron energies below ~ 200 keV, wave-particle interactions may begin to play a dominant role at higher energies (Miller et al 1997); 2) If wave particle interactions drive the evolution of the electron distribution, the relevant time scale is the electron diffusion time from the volume containing waves; 3) this time scale can have an energy dependence in the same sense as the Coulomb deflection time, yet operate on a much shorter time scale (e.g., Hamilton & Petrosian 1992).

5. Summary

Microwave emission associated with impulsive flares is dominated by nonthermal gyrosynchrotron emission from energetic electrons in coronal magnetic loops. This emission can be used to constrain a number of physical parameters, and their spatial and temporal evolution: the coronal magnetic field, the ambient thermal plasma, and the spatial and energy distribution of nonthermal electrons.

I have discussed one example of the diagnostic potential of microwave emission in greater detail: the uses of HXR/microwave timing to constrain transport and acceleration processes in impulsive flares. Obviously, such work may be taken much farther with appropriate observational inputs; namely, high resolution time series of images at multiple frequencies, with complementary HXR imaging and spectroscopic information.

References

Aschwanden MJ, Benz AO, Dennis BR, Schwartz RA. 1995b. *Astrophys. J.* 445:347
Aschwanden MJ, Wills MJ, Hudson HH, Kosugi T, Schwartz RA. 1996. *Astrophys. J.* 468:398
Aschwanden MJ, Bynum RM, Kosugi T, Hudson HS, Schwartz, RA. 1997. *Astrophys. J.* 487:936
Bai T, Ramaty R. 1979. *Astrophys. J.* 227:1072
Bai T, Dennis BR. 1985. *Astrophys. J.* 292:699
Bai T, Sturrock PA. 1989. *Annu. Rev. Astron. Astrophys.* 27:421
Bastian, T.S., Benz, A.O., Gary, D.E. 1998, ARAA 36, 131
Bastian, T.S., Aschwanden, M. J., Shibasaki, K. 1999, in preparation

Bastian, T.S., Aschwanden, M. J. 1999, in preparation

Bastian TS, Kiplinger A. 1991. *Max '91 Workshop #3*, Estes Park, CO, ed. R Winglee, A Kiplinger, p. 153

Cornell ME, Hurford GJ, Kiplinger AL, Dennis BR. 1984. *Astrophys. J.* 279:875

Crannell CJ, Frost KJ, Saba JL. Mätzler C, Ohki K. 1978. *Astrophys. J.* 223:620

Dennis BR. 1988. *Sol. Phys.* 118:49

Dulk GA. 1985. *Annu. Rev. Astron. Astrophys.* 23:169

Hamilton RJ, Petrosian V. 1992. *Astrophys. J.* 398:350

Hanaoka Y. 1996. *Sol. Phys.* 165:275

Hanaoka Y. 1997. *Sol. Phys.* 173:319

Kahler SW. 1977. *Astrophys. J.* 214:891

Kaufmann P, *et al* 1983. *Sol. Phys.* 84:311

Klein K-L. 1987. *Astron. Astrophys.* 183:341

Kosugi T, Dennis BR, Kai K. 1988. *Astrophys. J.* 324:1118

Kundu MR. 1961. *J. Geophys. Res.* 66:4308

Kundu MR, Nitta N, White SM, Shibasaki K, Enome S, et al. 1995. *Astrophys. J.* 454:522

Lee JW, Gary DE. 1994. *Sol. Phys.* 153:347

Miller JA, Cargill PJ, Emslie AG, Holman GD, Dennis BR, et al. 1997. *J. Geophys. Res.* 102, 14631

Nishio M, Yaji K, Kosugi T, Nakajima H, Sakurai T. 1997. *Astrophys. J.* , in press.

Preka-Papadema P, Alissandrakis CE. 1992. *Astron. Astrophys.* 257:307

Ramaty R. 1969. *Astrophys. J.* 158:753

Wang H, Gary DE, Lim J, Schwartz RA. 1994. *Astrophys. J.* 433:379

Wang H, Gary DE, Zirin H, Kosugi T, Schwartz RA, Linford G. 1995. *Astrophys. J. Lett.* 444:L115